International Journal of Modern Manufacturing Technologies
ISSN 2067–3604, Vol. XIV, No. 2 / 2022
https://doi.org/ 10.54684/ijmmt.2022.14.2.302

A NUMERICAL SOLUTION FOR THE ELASTIC SLIDING CONTACT WITH FRICTIONAL HEATING

Sergiu Spinu[1,2]

[1] Department of Mechanics and Technologies, Stefan cel Mare University of Suceava,
13th University Street, 720229, Romania
[2] Integrated Center for Research, Development and Innovation in Advanced Materials, Nanotechnologies, and Distributed Systems for Fabrication and Control (MANSiD), Stefan cel Mare University, Suceava, Romania

Corresponding author: Sergiu Spinu, sergiu.spinu@fim.usv.ro

Abstract: A thermoelastic contact model for non-conforming smooth or rough surfaces is proposed in this paper, based on a method for thermoelastic displacement computation. A classical contact model for the contact of rough surfaces is enhanced by integrating the thermal component of displacement. In the sliding contact model, heat is generated by friction at the contact surface, at a rate proportional to the sliding velocity, the frictional coefficient and the contact pressure. The latter, in its turn, is influenced by the initial clearance, the rigid body approach and the normal displacement, which comprises contributions from (1) the elastic displacement due to pressure, (2) the elastic displacement due to the shear tractions, assumed proportional to pressure according to Coulomb law of friction, and (3) the thermoelastic displacement due to the liberated heat, also proportional to pressure. These dependencies suggest that the geometric contact equation can be reduced to an equation in pressure, whose solution is obtained numerically based on an iterative search of the contact area and of the pressure distribution as in the case of isothermal contacts. A spherical contact is simulated with the newly advanced computer program, by including the thermoelastic effects. It is found that the contact area predicted by the isothermal contact model is larger than for the thermoelastic contact, and the pressure in the central contact region is underestimated when the thermal distortion is neglected. The advanced method is expected to provide base for the study of transient contact processes with consideration of thermal parameters.
Key words: thermoelastic contact, frictional heating, thermoelastic displacement, fast Fourier transform, convolution.

1. INTRODUCTION

Important machine elements such as gears or rolling bearings transmit load through non-conforming contacts that operate under severe conditions due to important stress gradients concentrated in a vicinity generally small compared to dimensions of the contacting bodies. Finding the contact area and the contact stresses arising in contacts between surfaces of general profiles (including rough surfaces) is one of the major challenges in contact mechanics. Moreover, when the mating surfaces slide relative to each other, a friction-related sharp temperature rise occurs at the contact interface, referred to as the flash temperature in tribology. Various contact failure modes such as scuffing, cracking or seizure are attributed to the frictional heating, and a combined elastic and thermal analyses may be required for accurate prediction of contact strength, fully taking into account the thermoelastic distortion of the contacting surfaces.
The complexity of the mathematical model describing the interactions involved in the thermoelastic contact led to a division in simpler submodels. The contact of general (rough) but isothermal solids has received great attention, and important research efforts concluded with a robust and efficient semi-analytical method that is orders of magnitude faster than a finite element simulation. Based on the conceptual strategy for the contact solution [1], efficient algorithms based on the Conjugate Gradient method were advanced [2,3]. Beside the efficiency of the numerical method for the solution of the linear system, a competent contact algorithm requires rapid methods for the displacement calculation, the most important candidates being the multi-level multi-summation [3,4], and the methods based on the fast Fourier transform (FFT) [5,6]. Comparative studies can be found in [7,8]. The contact algorithm advanced in [3], combined with the summation technique [6], is currently considered state-of-the-art and will also be applied in this paper.
On the other hand, thermoelastic stress and flash temperature analyses are mainly two-dimensional, and the heat sources are specified beforehand, without being derived from a contact process that takes into account the interactions between the contact and the thermoelastic effects. The study of the flash temperature in tribology pioneered with the

fundamental works of Blok [9] and Jaeger [10]. The thermoelastic contact between a rolling rigid indenter and a half-space with a surface-breaking crack exposed to a heat source induced by a Hertzian pressure distribution was analysed in [11], while these authors [12] investigated the surface temperature rise due to various imposed heat source shapes and different Peclet numbers. Gao et al. [13] advanced a transient flash temperature model for rough surfaces, in which heat partition was assessed with the aid of the FFT. Wang and Liu [14], and Liu and Wang [15], were the first to develop two-dimensional contact models for rough surfaces that take into account the mechanical response to load and the steady-state thermal phenomena, as well as the interaction between them. An extension to the three-dimensional case was later achieved [16] with the aid of FFT techniques.

This paper advances a numerical formulation that integrates state-of-the-art techniques for contact solution and displacement computation, by considering the coupled effect of pressure, of shear tractions and of thermoelastic distortion. The contact variables are obtained under a full integration between the thermal phenomena and the mechanical response to contact load. This type of analysis is expected to provide a more realistic simulation tool for the prediction of the load carrying capacity of the thermoelastic contact.

2. CONTACT PROBLEM MODEL

The contact between two elastic bodies convex in the contact region, i.e., a non-conforming (or concentrated) contact, can be modelled by a so-called equivalent contact [1] between an equivalent rigid punch and an equivalent half-space whose elastic parameters are chosen so that the contact compliance remains unchanged:

$$\frac{1}{E^*}=\frac{1-\nu_1^2}{E_1}+\frac{1-\nu_2^2}{E_2}, \qquad (1)$$

with E_i and ν_i, $i=1,2$ the Young modulus and the Poisson's ratio of the contacting materials. The new defined elastic parameter for the half-space, E^*, is also referred to as the equivalent Young modulus of the contact. Practically, the combined contact geometry of the two bodies is attributed exclusively to the indenter, whereas the contribution of the elastic properties of the contacting materials is considered exclusively for the equivalent half-space. When frictional heating is considered in a sliding contact, the equivalent punch is assumed adiabatic, whereas the heat generated by friction is conducted in the equivalent half-space. With these assumptions, the word "equivalent" will be omitted from now on for simplicity. The problem of a punch sliding with a velocity v on a stationary half-space, can be treated as an equivalent problem in which the indenter is fixed and the half-space is mobile. This assumption converts a problem model having time t as a parameter in a simpler problem in which the time parameter is substituted by a position parameter $x=vt$. However, in the model developed in this paper, the contact is assumed quasi-stationary, meaning the time parameter is not needed in the thermal analyses, and all model parameters are independent of time. Such an assumption holds only for small Peclet numbers, where the latter parameter denotes [1] the ratio of the speed of the half-space to the rate of diffusion of heat into the half-space.

The solution of the contact problem is expected to assess contact interface distributions such as the contact pressure, the contact area, temperature rise or the gap between the contacting surfaces. The main step for achieving this solution is the displacement computation of the elastic half-space. The half-space assumption, which allows treating the contacting bodies as elastic half-spaces, stands at the base of the mathematical formulation. Fundamental results derived in the theory of linear elasticity can thus be implemented in the contact problem model to assess the needed displacements. The use of half-space assumption for a non-conforming contact is justified giving that the gradients of elastic stresses, as well as the temperature gradients which introduce thermal distortion and stress, are significantly large only in a vicinity of the contact region. Giving that the contact region is small compared to the magnitude of the bulk bodies, the limiting surfaces can be approximated as plane in the contact region. The bulk of the bodies may experience global changes in temperature, but these only lead to relatively uniform expansion or contraction that does not produce additional thermal stresses, and thus does not significantly modify the contact zone.

The contact problem is reported to a cartesian coordinate system with the origin in the initial point of contact, and the x_1x_2 plane coincides with the half-space boundary. The normal (i.e., along direction of x_3, normal to the half-space boundary) displacement field of the elastic half-space dictates the extension of the contact zone, i.e., the contact area, and the pressure distribution on it. In a sliding contact, the displacement comprises contributions from three sources: (a) the pressure distribution $p(x_1,x_2)$, (b) the shear tractions $s(x_1,x_2)$, and (c) the steady-state heat flux $\dot{h}(x_1,x_2)$ generated by friction. However, these three sources are not independent: the shear traction is related to pressure by Coulombian friction:

$$s(x_1,x_2)=\mu p(x_1,x_2), \quad (2)$$

whereas the heat rate liberated by friction is also proportional to pressure [1]:

$$\dot{h}(x_1,x_2)=\mu v p(x_1,x_2), \quad (3)$$

where μ is the frictional coefficient, assumed uniform on the contact area. In all three cases, the solutions for point forces or point sources of heat acting on the elastic half-space boundary, i.e., the Green's functions $G^p(x_1,x_2), G^s(x_1,x_2)$ and $G^h(x_1,x_2)$, are available in closed form in the literature [1]. Integration of these fundamental functions give the three components of the normal displacement:

$$u_3(x_1,x_2)=u_3^p(x_1,x_2)+u_3^s(x_1,x_2)+u_3^h(x_1,x_2), \quad (4)$$

where:

$$u_3^p(x_1,x_2)=\int_{-\infty}^{\infty}\int_{-\infty}^{\infty} G^p(x_1-x_1',x_2-x_2')p(x_1',x_2')dx_1'dx_2', \quad (5)$$

$$u_3^s(x_1,x_2)=\int_{-\infty}^{\infty}\int_{-\infty}^{\infty} G^s(x_1-x_1',x_2-x_2')s(x_1',x_2')dx_1'dx_2', \quad (6)$$

$$u_3^h(x_1,x_2)=\int_{-\infty}^{\infty}\int_{-\infty}^{\infty} G^h(x_1-x_1',x_2-x_2')\dot{h}(x_1',x_2')dx_1'dx_2', \quad (7)$$

$$G^s(x_1,x_2)=x_1/(\pi G^*(x_1^2+x_2^2)), \quad (8)$$

$$G^p(x_1,x_2)=1/(\pi E^*\sqrt{x_1^2+x_2^2}), \quad (9)$$

with G^* is the equivalent share modulus:

$$\frac{1}{G^*}=\frac{(1+\nu_1)(1-2\nu_1)}{2E_1}-\frac{(1+\nu_2)(1-2\nu_2)}{2E_2}. \quad (10)$$

The Green's function for the thermal displacement $G^h(x_1,x_2)$ was discussed in [17]. The double integrals (5), (6) and (7) have the same structure and are in fact double convolution products. If the symbol "$\otimes$" is used to denote the continuous convolution operation, relation (4) can be written as:

$$u_3=G^p\otimes p+G^s\otimes s+G^h\otimes\dot{h}, \quad (11)$$

which, together with (2) and (3) yields:

$$u_3=\left(G^p+\mu G^s+\mu\nu G^h\right)\otimes p. \quad (12)$$

The latter equation suggests that the normal displacement in a sliding contact with consideration of frictional heating can be expressed in terms of pressure, frictional coefficient, sliding velocity and the appropriate Green's functions for the elastic half-space. A classical contact model [1, 3] can be further implemented, consisting in the following boundary conditions:

(A) On the contact area, there exist no clearance between the contacting surfaces, thus, from geometrical considerations:

$$r(x_1,x_2)=u_3(x_1,x_2)+z(x_1,x_2)-\delta=0, \quad (13)$$

with $z(x_1,x_2)$ the punch geometry in undeformed state and δ the rigid-body approach, i.e., the approach between points in the contacting bodies distant from the contact region. Relation (13) expresses that the indenter does not penetrate into elastic half-space, thus r cannot be negative. Moreover, pressure is assumed strictly positive on the contact area, $p(x_1,x_2)>0$, which neglects adhesion effects but provide means to achieving an iterative solution to the contact model, as shown in the next section. Heat is only liberated on the contact area, as suggested by equation (3).

(B) Outside the contact area, there exist a clearance between the surfaces, thus $r(x_1,x_2)>0$, the pressure vanishes, $p(x_1,x_2)=0$, and no heat is generated or conducted into the half-space (the clearance acts as an insulator).

The solution of the contact model is discussed in the following section.

3. NUMERICAL SOLUTION

As stated in [1], a closed-form solution for the contact between elastic bodies of general profiles cannot be easily achieved because the pressure distribution and the contact area are both unknown. One notable exception is the Hertz contact, but the defining assumptions for the latter are too strong for the contact scenario considered in this paper. The numerical iterative solution advanced in [3], which is the state-of-the-art in computational contact mechanics, can also be used for the contact model developed in this paper. The contact area and the pressure distribution are found by trial-and-error. A computational domain expected to contain the contact area is the initial approximation. Equation (13) is solved on the latter domain, giving a pressure solution that contains both positive and negative values. In the next iteration, the contact area is adjusted to include only regions with

positive pressure, and equation (13) is solved again, giving a new and improved pressure distribution (which contains lesser negative values). The process is repeated until a contact area is found that verifies the following conditions: (a) solving equation (13) on it only yields positive pressure, and (b) the computed pressure verifies the static force equilibrium. The found solution is a valid solution of the elastostatic boundary value problem. Based on the theorem of unicity of solution in elastostatics, the found solution is the required one. This paper extends the contact model [3] by adding the frictional effects. Here the contributions of the frictional shear and of the frictional heating to the normal displacement are accounted for. Moreover, the DCFFT technique [6] applied to convolutions computations provides further computational efficiency and precision.

Solution of equation (13) is achieved based on the condition that the boundary conditions are verified in a set of discrete points instead of in a continuum. Good candidates for such control points are the centers of elementary cells in a rectangular mesh imposed in the half-space boundary around the initial point of contact. The discretized domain automatically becomes the problem computational domain, and integrals (5) - (7) are substituted by double-summations on a finite range. The consideration of the control points assumes that the value of every problem parameter in a control point is representative for the whole elementary cell. Thus, each two-dimensional distribution will be represented by a matrix of elements, and equation (13) will turn into a linear system having the pressure matrix as unknown. The convolutions (5) - (7) will be replaced in the discrete model by multi-summations:

$$u_3^p(x_{1i},x_{2j})=\sum_{k=1}^{N_1}\sum_{\ell=1}^{N_2}D^p(x_{1i}-x_{1k},x_{2j}-x_{2\ell})\,p(x_{1k},x_{2\ell}), \tag{14}$$

$$u_3^s(x_{1i},x_{2j})=\sum_{k=1}^{N_1}\sum_{\ell=1}^{N_2}D^s(x_{1i}-x_{1k},x_{2j}-x_{2\ell})\,s(x_{1k},x_{2\ell}), \tag{15}$$

$$u_3^h(x_{1i},x_{2j})=\sum_{k=1}^{N_1}\sum_{\ell=1}^{N_2}D^h(x_{1i}-x_{1k},x_{2j}-x_{2\ell})\,\dot{h}(x_{1k},x_{2\ell}) \tag{16}$$

that can be regarded as discrete convolutions products (operation denoted by the symbol "$\square$"), giving a discrete counterpart of (11) and (12):

$$\begin{aligned} u_3 &= D^p \square\ p + D^s \square\ s + D^h \square\ \dot{h} = \\ &= \left(D^p + \mu D^s + \mu V D^h\right) \square\ p. \end{aligned} \tag{17}$$

In relations (14) - (16), x_{mn} is the coordinate of the control point attached to the n^{th} elementary cell in the direction of $\vec{x}_m$, $m=1,2$; $N_m, m=1,2$ is the number of control points in the direction of $\vec{x}_m$, and D^m, $m=p,s,\dot{h}$ are the influence coefficients for the three considered types of sources: pressure, shear and frictional heat. $K^m(x_{1i}-x_{1k},x_{2j}-x_{2\ell})$ expresses the contribution of a unity source uniformly distributed on the elementary cell centered in the control point of coordinates $(x_{1k},x_{2\ell})$, to the control point (x_{1i},x_{2j}), i.e., the observation point. Relations (14) - (16) imply that in the superposition effort, each control point in the established mesh is considered as both source point and observation point. From the description given above, the influence coefficients are in fact the double integrals of the Green's functions $G^m(x_1,x_2)$. The derivation of D^h is detailed in [17]. In the same manner, with the notations $x_{iu}=x_i+\Delta_i$, $x_{i\ell}=x_i-\Delta_i$, $i=1,2$, $2\Delta_i$ being the distance along $\vec{x}_i$ between two adjacent control points, the influence coefficients for pressure and shear can be computed from:

$$\begin{aligned} D^m(x_1,x_2) &= g^m(x_{1u},x_{2u})+g^m(x_{1\ell},x_{2\ell})-\ldots \\ &-g^m(x_{1u},x_{2\ell})-g^m(x_{1\ell},x_{2u}), \quad m=p,s, \end{aligned} \tag{18}$$

$$g^p(x_1,x_2)=\frac{1}{\pi E^*}\begin{pmatrix} x_1\ln\left(x_2+\sqrt{x_1^2+x_2^2}\right)+\ldots \\ +x_2\ln\left(x_1+\sqrt{x_1^2+x_2^2}\right)\end{pmatrix}, \tag{19}$$

$$g^s(x_1,x_2)=\frac{1}{\pi G^*}\left(\frac{x_2}{2}\ln(x_1^2+x_2^2)-x_2+x_1\operatorname{atan}\left(\frac{x_2}{x_1}\right)\right). \tag{20}$$

It should be noted that the function g^p from (19) and its counterpart for the calculation of temperature rise $g^{\Delta T}$, derived in [17], can be obtained one from the other by interchanging the constants $1/E^*$ and $1/(2K)$, with K the conductivity of the material.

The developed digitized model allows for the calculation of the normal displacement (17) for arbitrary pressure p and thus can be used in the iterative scheme [3] that finds the contact area and the pressure distribution in the thermoelastic elastic contact between bodies of arbitrary profiles. The developed contact model can equally be used for rough contact problems, provided in equation (13) the initial

contact geometry $z(x_1, x_2)$ is substituted by a discrete matrix of coordinates obtained by measuring with optical profilometry an engineering surface. The use of the DCFFT technique [6] assures that the best available computational efficiency is attained. The algorithm can handle detailed roughness information containing a large number of individual coordinates.

One particular feature of the current model is that, whereas the absolute values of u^p and u^s can be derived as described in this section, u^h depends upon a reference point, as shown in [17]. Therefore, the total displacement will in its turn depend upon the chosen datum. The influence of the reference point will manifest itself as a constant on the whole computational domain. However, this is not an issue for the contact solver [3]. Indeed, in the numerical formulation, the rigid body approach δ from equation (13) is derived as the average value of the sum $u_3(x_1, x_2) + z(x_1, x_2)$. The gap $r(x_1, x_2)$ from the same relation is in fact the residual of the linear system to be solved. Adding a constant to the displacement field $u_3(x_1, x_2)$ will not impact the residual $r(x_1, x_2)$, as the said constant will be balanced through the subtraction of δ. In other words, the contact solver works in such a way that relative values of displacement on the computational domain are enough to derive the contact area and the pressure distribution. However, the rigid body approach δ will not be available from the current model. The performance of the contact is mostly impacted by the stress state developed in the contacting body, which is related to the contact tractions, and therefore in most contact situations the lack of information on the rigid body approach may not be an issue.

4. RESULTS AND DISCUSSIONS

A numerical simulation is performed with the developed contact model. A spherical punch, rigid and adiabatic, is pressed against an elastic and conductive half-space. The contact parameters according to the Hertzian framework, i.e., a frictionless and isothermal contact, are used as reference: the contact radius a_H for coordinates, the central pressure p_H for pressure and the rigid-body approach δ_H for displacement. The elastic parameters of the half-space are fixed: the Young modulus $E = 210$ GPa, the Poisson's ratio $\nu = 0.3$, whereas the thermal parameters are chosen as: the thermal conductivity $K = 50.2$ W/(m·°K), and the distortivity 0.303 μm/W.

The frictional coefficient is uniform over the contact area and constant in time, $\mu = 0.2$. The punch slides over the half-space from left to right with a speed $v = 0.25$ m/s.

The individual modules for the calculation of displacements due to pressure and shear tractions are first benchmarked against existing closed-form solutions. The normal displacement due to a Hertzian pressure can be expressed as [1]:

$$u_H^p(r) = \begin{cases} \pi p_H (2a_H^2 - r^2)/(2E^* a_H), & |r| < a_H; \\ p_H \left[(2a_H^2 - r^2)\sin^{-1}(a_H/r) + r a_H \sqrt{1-(a_H/r)^2} \right] \Big/ (a_H E^*), & |r| \geq a_H, \end{cases} \quad (21)$$

whereas that due to the shear tractions $s(r) = 1/\sqrt{1-(r/a_H)^2}$ is given by:

$$u^s(r) = -\frac{2a_H(a_H - \sqrt{a_H^2 - r^2})}{G^* r}, \quad |r| \leq a_H. \quad (22)$$

The distributions in relations (21) and (22) are precisely reproduced by the computer program, as depicted in figure 1. The solution of the thermoelastic sliding contact is then obtained with the aforementioned elastic and thermal parameters. The resulting pressure and displacement profiles in the plane $x_2 = 0$ are depicted in figures 2 and 3.

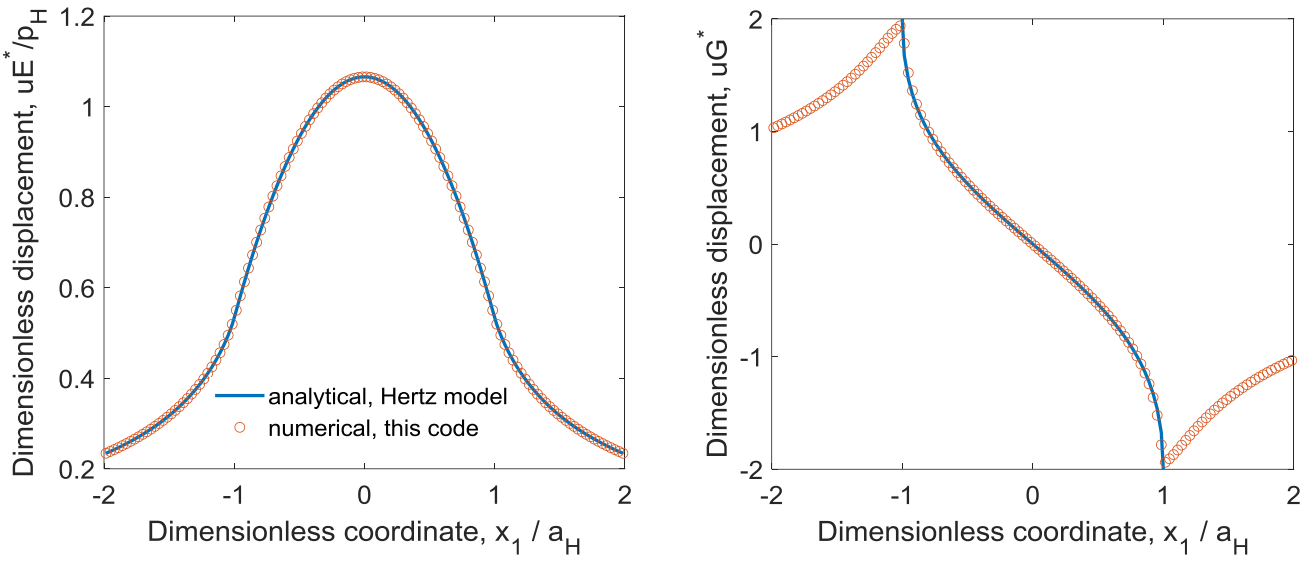

Fig.1. Normal displacement due to: a) Hertzian pressure; b) imposed shear.

Figure 2 suggests that, when only u_3^p is considered in equation (4), the resulting pressure profile match well the Hertzian semi-elliptical distribution. The distribution symmetry is lost when u_3^s is also added, as the pressure peak and the center of the contact area are shifted toward the trailing edge of the contact. Superimposing the thermal displacement u_3^h results in a contraction of the contact area and in an increase of the peak pressure. The magnitude of the shift depends on the frictional coefficient, whereas the thermal effect also depends on the sliding speed.

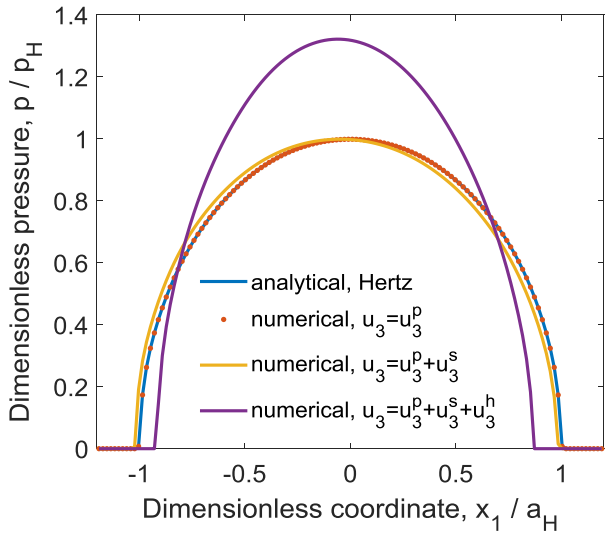

Fig. 2. Influence of displacement on the pressure profiles in the thermoelastic contact.

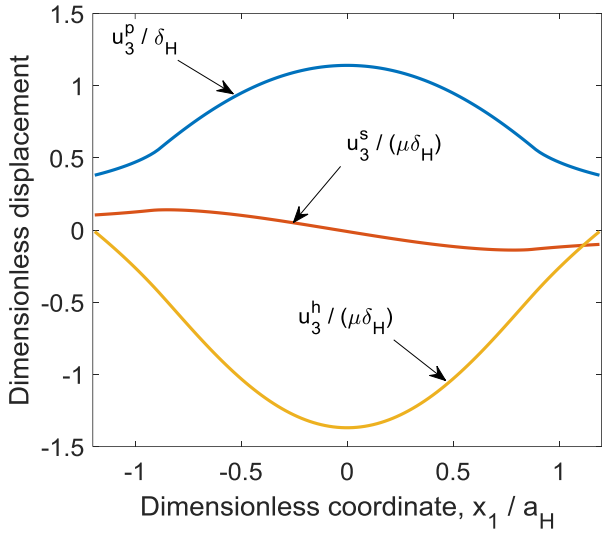

Fig. 3. Components of displacement in the thermoelastic contact.

Figure 3 clearly shows that is u_3^p and u_3^h are both symmetrical, but u_3^p is concave, increasing the contact conformity, whereas u_3^h is convex, decreasing the contact conformity and thus reducing the contact area and increasing the peak pressure. The numerical simulation suggests that the thermal effect increases the contact severity and therefore should be considered for competent tribological design.

5. CONCLUSIONS

The solution of the sliding contact problem is obtained in this paper without the limiting assumption of an isothermal contact, present in most contact models. The consideration of thermal effects is facilitated by the numerical technique for the calculation of

thermoelastic displacement due to arbitrary steady heat flux.

The normal displacement is calculated by considering contributions from the contact tractions, pressure and shear, as well as from the steady-state heat generated by friction. The geometric contact equation reduces to an equation having the pressure distribution as unknown. Digitization of a plane domain around the initial point of contact further transforms the equation into a linear system whose solution is pursued iteratively. This approach is made possible by the technique for displacement computation, allowing for arbitrary pressure input.

Although the thermoelastic displacement is only obtained with respect to a reference point, contact parameters such as the contact area and the pressure distribution are obtained. The numerical simulation suggests that the assumption of an isothermal contact seriously underestimates the maximum contact pressure and thus the contact severity. The contact area predicted by the thermoelastic contact model is smaller than the one obtained from the isothermal model, although the increase in pressure suggests that an elastic-plastic analysis would be more appropriate for rough surfaces.

Integration of thermal information in the contact models is expected to improve the design of mechanical contacts and to reduce the damage of machine components due to contact failure.

6. REFERENCES

1. Johnson K. L., (1996), *Contact Mechanics* (Cambridge: University Press).
2. Nogi T., Kato T., (1997), *Influence of a hard surface layer on the limit of elastic contact: Part I—Analysis using a real surface model*, ASME J. Tribol., 119, 493–500.
3. Polonsky I, A., Keer L. M., (1999), *A new numerical method for solving rough contact problems based on the multi-level multi-summation and conjugate gradient technique*, Wear, 231, 206–219.
4. Lubrecht A, A., Ioannides E., (1991), *A fast solution of the dry contact problem and the associated subsurface stress-field using multilevel techniques*, ASME J. Tribol., 113, 128–133.
5. Polonsky I. A., Keer L. M., (2000), *A fast and accurate method for numerical analysis of elastic layered contacts*, ASME J. Tribol., 122, 30–35.
6. Liu S., Wang Q., Liu G., (2000), *A versatile method of discrete convolution and FFT (DC-FFT) for contact analyses*, Wear, 243(1-2), 101–111.
7. Polonsky I. A., Keer L. M., (2000), *Fast methods for solving rough contact problems: A comparative study*, ASME J. Tribol., 122, 36–41.
8. Allwood J. M., (2005), *Survey and performance assessment of solution methods for elastic rough contact problems*, ASME J. Tribol., 127, 10-23.
9. Blok H., (1937), *Theoretical study of temperature rise at surfaces of actual contact under oiliness lubricating conditions*, Proc. General Discussion on Lubrication and Lubricants, London, 2, Institution of Mechanical Engineers, London, 222–235.
10. Jaeger J. C., (1942), *Moving sources of heat and the temperature at sliding contacts*, Proc. R. Soc. New South Wales, 76, 203–224.
11. Goshima T., Keer L. M., (1990), *Thermoelastic contact between a rolling rigid indenter and a damaged elastic body*, ASME J. Tribol., 112, 382–391.
12. Tian X., Kennedy F. E., (1994), *Maximum and average flash temperatures in sliding contacts*, ASME J. Tribol., 116, 167–173.
13. Gao J. Q., Lee S. C., Ai X. L., (2000), *An FFT-based transient flash temperature model for general three-dimensional rough surface contacts*, ASME J. Tribol., 122, 519–523.
14. Wang Q., Liu G., (1999), *A thermoelastic asperity contact model considering steady-state heat transfer*, STLE Tribol. Trans., 42(4), 763–770.
15. Liu G., Wang Q., (2000), *Thermoelastic asperity contacts, frictional shear, and parameter correlations*, ASME J. Tribol., 122, 300–307.
16. Liu G., Wang Q., (2000), *A three-dimensional thermomechanical model of contact between non-conforming rough surfaces*, ASME J. Tribol., 123, 17–26.
17. Spinu S., (2022), *Thermoelastic displacement and temperature rise in a half-space due to a steady-state heat flux*, Int. J. of Mod. Manufact. Technol., 14(3), 326-332.

Received: May 11, 2022 / Accepted: December 15, 2022 / Paper available online: December 20, 2022